THE JOURNAL OF PHYSICAL CHEMISTRY A

Article

pubs.acs.org/JPCA

Electron Inelastic Mean Free Path Theory and Density Functional Theory Resolving Discrepancies for Low-Energy Electrons in Copper

C. T. Chantler* and J. D. Bourke

School of Physics, University of Melbourne, Parkville, Vic 3010, Australia

ABSTRACT: We develop the many-pole dielectric theory of UV plasmon interactions and electron energy losses, and couple our advances with recent developments of Kohn−Sham density functional theory to address observed discrepancies between high-precision measurements and tabulated data for electron inelastic mean free paths (IMFPs). Recent publications have demonstrated that a five standard error difference exists between longstanding theoretical calculations and measurements of electron IMFPs for elemental solids at energies below 120 eV, a critical region for analysis of electron energy loss spectroscopy (EELS), X-ray absorption spectroscopy (XAS), and related technologies. Our implementation of improved optical loss spectra and a physical treatment of second-order excitation lifetimes resolves this problem in copper for the first time for energies in excess of 80 eV and substantially improves agreement for lower energy electrons.

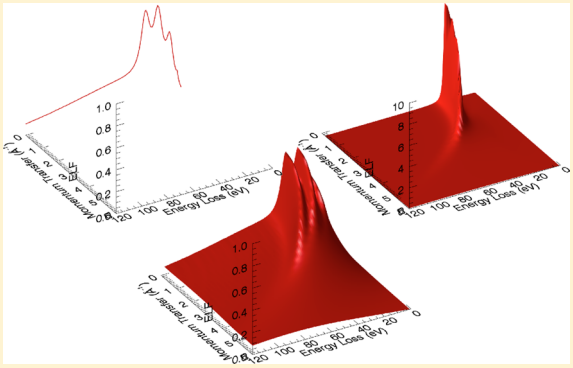

INTRODUCTION

The relative electric permittivity, or complex dielectric function ε, is one of the most fundamental and important parameters in solid state physics and the principal quantifier of the response of a solid material to an external electric field. Importantly, the dielectric function is readily transformed into an energy loss function, or ELF, that represents the probability of a material absorbing energy $\hbar\omega$ and momentum $\hbar q$ from an energetic incoming particle such as a photon or an electron. The ELF is defined by

$$\mathrm{Im}\left[\frac{-1}{\varepsilon(q,\omega)}\right] = \frac{\varepsilon_2(q,\omega)}{\varepsilon_1(q,\omega)^2 + \varepsilon_2(q,\omega)^2} \quad (1)$$

where $\varepsilon_1(q,\omega)$ and $\varepsilon_2(q,\omega)$ are the real and imaginary parts of the dielectric function, respectively. These parameters are also directly obtained from the complex refractive index $n + ik$ following $\varepsilon_1 = n^2 - k^2$ and $\varepsilon_2 = 2nk$. In the optical limit, corresponding to the case where $q \to 0$, these parameters can be obtained experimentally using optical reflection or transmission measurements or less directly using techniques such as reflection electron energy loss spectroscopy (REELS). Extensive tabulations[1] and compilations[2] are widely cited by authors looking to interpret a wide range of experimental data, particularly in spectroscopy[3−5] and imaging.[6]

Theoretical determinations of optical parameters are available but are difficult to derive for low energies below a few hundred electronvolts. Low energy electron inelastic mean free paths (IMFPs) have been the concern of recent publications because of their importance to the field of X-ray absorption fine structure (XAFS),[7,8] a spectroscopic tool used for nanoscale structural determinations. XAFS has wide-ranging applicability to elemental crystals,[9] solutions,[10] amorphous materials, and catalytic active centers.[11] However, analysis of XAFS spectra is often limited, particularly in the information-rich low-energy region, by a lack of accurate data concerning the electron IMFP.[12]

Established theoretical approaches appear to overestimate the IMFP for energies less than ∼100 eV.[7,8,13] This situation has led to a critical re-evaluation of the commonly used optical data model, which represents energy loss spectra in terms of lossless Lindhard or Drude−Lorentz functions. In the Lindhard case this modeling is well constrained; however, the representation of plasmon excitations as delta functions is necessarily unphysical. Mermin type functions and corresponding implementations of second-order (excitation) lifetimes not only produce a more realistic model but also significantly improve the agreement with experiment for copper.[14]

Many-pole dielectric models typically rely on experimental optical ELFs,[15−17] which usually provide no estimates of uncertainties[1,2] and in many cases show poor agreement with one another.[18] The latest theory utilizing such data[14,19] remains discrepant from experimental copper IMFP results from XAFS by at least 5 standard errors at 120 eV.[14] The disagreement is worse for lower energies. We are therefore motivated to investigate the applicability of density functional theory (DFT) to low-energy optical loss data to improve our understanding of this fundamental component of electron inelastic scattering theory.

Received: August 22, 2013
Revised: January 22, 2014
Published: January 22, 2014

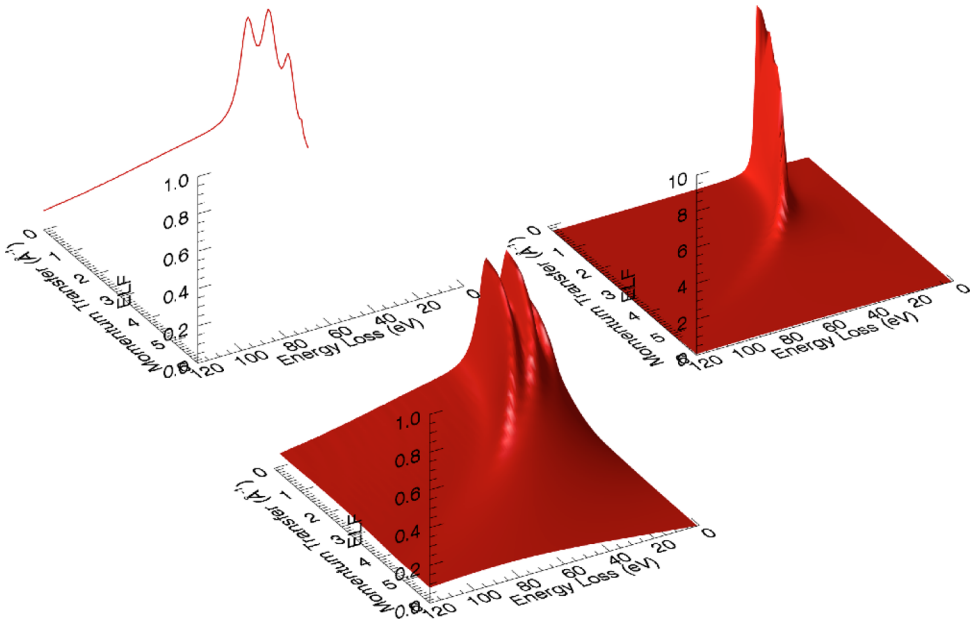

Figure 1. Components used to construct the electron energy loss function. On the left is an externally determined optical loss function,[1] corresponding to Im$[-1/(\varepsilon(0,\omega))]$. The right plot shows a one-component Lindhard ELF, while the bottom plot is a summation of Lindhard ELFs that reproduce the original plot in the optical limit.

THEORY

DFT is a computational technique developed by Hohenberg and Kohn[20] to determine electron eigenstates in a solid where electron−electron and other interactions give rise to an intractable number of terms in the Schrödinger equation. The technique involves a number of approximations and simplifications,[21] but with respect to solid-state physics is most succinctly described in terms of the Kohn−Sham equation:[22]

$$\left(-\frac{\hbar}{2m}\nabla^2 + V_{\mathrm{Ne}} + V_{\mathrm{ee}} + V_{\mathrm{xc}}\right)\psi = E\psi \tag{2}$$

where the potential components correspond to the nuclear−electron interactions (V_{Ne}), electron−electron interactions (V_{ee}), and exchange and correlation (V_{xc}). Interaction potentials may be described in terms of functions of local charge densities, rather than by consideration of individual particles, enabling the problem to be treated with finite resources. The computational package WIEN2k has been developed to solve the Kohn−Sham equation via a recursive self-consistent field algorithm.[23] The basis eigenfunctions take the form of radial functions multiplied by spherical harmonics in regions close to atomic cores, while in interstitial regions linearized augmented plane waves (LAPW) are used. The exchange and correlation potential is determined following the generalized gradient approximation described by Perdew et al.[24]

Calculation of Kohn−Sham eigenstates allows the user to probe physical and chemical properties of periodic materials. Ambrosch−Draxl and Sofo[25] have demonstrated that WIEN2k packages can be extended to calculate low-energy dielectric functions and optical energy-loss data. The momentum matrix elements are given by

$$M_{n',n}(\mathbf{k}, \mathbf{q}) = \langle n', \mathbf{k}|e^{-i\mathbf{q}\mathbf{r}}|n, \mathbf{k} + \mathbf{q}\rangle \tag{3}$$

These amplitudes can be used in conjunction with the free-electron gas theory of Lindhard to determine the response of a solid to optical excitations. The Lindhard theory generalizes the dielectric behavior of a homogeneous gas of electronic charge in response to an external perturbation, and provides an expression for the electric permittivity:[26]

$$\varepsilon_{\mathrm{L}}(q, \omega) = 1 + \frac{4\pi e^2}{q^2}\sum_{\mathbf{k}}\frac{f^0(\mathbf{k}) - f^0(\mathbf{k}+\mathbf{q})}{E(\mathbf{k}+\mathbf{q}) - E(\mathbf{k}) - \hbar\omega} \tag{4}$$

where f^0 is the Fermi distribution. The Lindhard model is rigorous for a lossless free electron gas. In a solid, however, excitations are limited by the complex band structure of the material, which is characterized by the transition amplitudes $M_{n',n}(\mathbf{k},\mathbf{q})$. Following Ambrosch−Draxl and Sofo,[25] we write the dielectric function in the optical limit as a modulation of the Lindhard expression:

$$\varepsilon(0, \omega) = 1 + \lim_{q\to 0}\left\{\frac{4\pi e^2}{q^2}\sum_{n,n',k}\frac{f^0(\mathbf{k}) - f^0(\mathbf{k}+\mathbf{q})}{E(\mathbf{k}+\mathbf{q}) - E(\mathbf{k}) - \hbar\omega}|M_{n,n'}(\mathbf{k}, \mathbf{q})|^2\right\} \tag{5}$$

The case $n = n'$ represents intraband optical transitions, while $n \neq n'$ gives the interband contribution. This formalism is implemented into WIEN2k to compute the imaginary part of the optical dielectric function, $\varepsilon_2(0,\omega)$. The real part, $\varepsilon_1(0,\omega)$, is then determined by a Kramers−Kronig transformation,[23,25] enabling determination of the optical ELF Im$[-1/(\varepsilon(0,\omega))]$.

Recently, Werner et al.[18] published optical energy loss data evaluated for a variety of elemental solids at energies up to 70 eV and transformed these into electron energy-loss data, from which the authors were able to make calculations of low-energy IMFPs. This promising study was based upon the classical Drude approximation and, ergo, necessarily misrepresents the momentum-dependence of the electron ELF. Here we implement a more rigorous Lindhard partial pole model, and then explicitly consider the impact of plasmon broadening on the electron ELF and IMFP.[14]

dx.doi.org/10.1021/jp408438r | J. Phys. Chem. A 2014, 118, 909−914

To do this we must extend the optical ELF into the finite-q region to describe the behavior of electrons depositing significant momentum $\hbar q$ into the system. We initially present a partial-pole model similar to the full Penn algorithm for IMFP determination.[27] This model was originally inspired by the early work of Tung et al., who invoked the statistical approximation to suggest a model of the dielectric response of a condensed matter system comprising a summation of noninteracting component oscillators.[28] In the current model, discrete plasmon resonances are represented as summations of partial excitations using Lindhard functions.[26]

When applied to the optical ELF, the Lindhard dielectric function produces a singularity at a defined frequency ω_p known as the plasma frequency, which is principally determined by the charge density of the material:

$$\mathrm{Im}\left[\frac{-1}{\varepsilon_L(0,\omega)}\right] = \frac{\pi}{2\omega}\delta(\omega-\omega_p) \tag{6}$$

Applying this to a solid, we may consider the optical ELF to be composed of Lindhard terms with closely spaced plasma frequencies ω_i such that

$$\mathrm{Im}\left[\frac{-1}{\varepsilon(0,\omega)}\right] = \sum_i \frac{A_i\pi}{2\omega}\delta(\omega-\omega_i) \tag{7}$$

We can define the amplitude parameters, A_i, so that the optical ELF matches that determined via WIEN2k. Explicitly,

$$\mathrm{Im}\left[\frac{-1}{\varepsilon_{DFT}(0,\omega)}\right] = \sum_i A_i \mathrm{Im}\left[\frac{-1}{\varepsilon_L(0,\omega;\omega_p=\omega_i)}\right] \tag{8}$$

$$= \sum_i \frac{A_i\pi}{2\omega}\delta(\omega-\omega_i) \tag{9}$$

With these amplitude parameters determined, we can build a momentum-dependent ELF following the natural q-dependence of the Lindhard expression:

$$\mathrm{Im}\left[\frac{-1}{\varepsilon(q,\omega)}\right] = \sum_i A_i \mathrm{Im}\left[\frac{-1}{\varepsilon_L(q,\omega;\omega_p=\omega_i)}\right] \tag{10}$$

In practice this requires a particularly dense grid of ω_i values to ensure numerical precision. For this study we utilize a pole spacing of approximately 0.03 eV in order to achieve acceptable convergence in the ELF, while sampling of the spectrum is carried out every 0.005 eV to ensure numerical stability. Figure 1 visualizes the procedure by which these components form the total ELF. On the left, the ELF for copper is plotted in the optical limit. The plot on the right shows a single-component Lindhard ELF with a small amount of broadening added for visibility. Summation of such Lindhard curves with appropriate relative magnitudes and optical peak positions allows for the construction of an ELF, as shown in the bottom plot, that is correct in the optical limit and extended in a well-constrained manner to the region of finite momentum transfer.

With the momentum-dependent ELF determined, we can calculate the electron IMFP following the well-known relationship[15]

$$\lambda^{-1}(E) = \frac{\hbar}{a_0\pi E}\int_0^{E-E_F/\hbar}\int_{q_-}^{q_+}\frac{1}{q}\mathrm{Im}\left[\frac{-1}{\varepsilon(q,\omega)}\right]\mathrm{d}q\mathrm{d}\omega \tag{11}$$

where the $q_\pm$ limits are given kinematically by

$$q_\pm = \sqrt{\frac{2mE}{\hbar^2}} \pm \sqrt{\frac{2m}{\hbar^2}(E-\hbar\omega)} \tag{12}$$

The form of the $q_\pm$ limits coupled with the $1/q$ coefficient conspire to exaggerate the impact of the very low-energy region of the ELF on the electron IMFP. A consequence of this effect is that any broadening mechanism introduced into the Lindhard components will increase the low-energy losses and thus cause a significant decrease in the IMFP at the energies of interest in this work (but will have negligible effect at very high energies due to the large range of integration). The implementation of broadening is physically demanded due to the finite lifetimes of the plasmon and single-electron excitations represented by the resonance peaks in the ELF and may be accomplished by generalizing the lossless Lindhard dielectric function into the Mermin function given by[29]

$$\varepsilon_M(q,\omega) = 1 + \frac{(1+i\gamma/\omega)[\varepsilon_L(q,\omega+i\gamma)-1]}{1+(i\gamma/\omega)[\varepsilon_L(q,\omega+i\gamma)-1]/[\varepsilon_L(q,0)-1]} \tag{13}$$

where γ is a broadening term induced by the excitation lifetime $\tau = 1/\gamma$. $\varepsilon_M(q,\omega)$ may be used in place of $\varepsilon_L(q,\omega)$ in eq 10; however, the matching condition of eq 8 becomes unconstrained, with many sets of parameters A_i, ω_i, and γ_i potentially allowing for acceptable agreement with the optical spectrum. As a result, we approximate the IMFP reduction due to plasmon broadening following the results of a previous analysis[14] that utilized Mermin terms with independently determined parameters for elemental copper.[17]

RESULTS

Figure 2 shows the optical ELF of copper calculated via WIEN2k over 0−120 eV, along with commonly cited

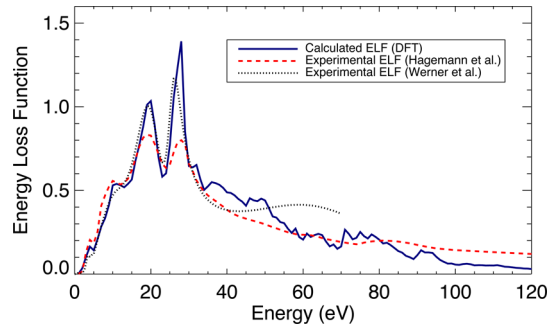

Figure 2. Optical energy loss function of copper determined using density functional theory as implemented by the WIEN2k package. Also shown is experimental data from optical transmission measurements by Hagemann et al.[1] and REELS analysis from Werner et al.[18]

experimental results from Hagemann et al.,[1] and more recent experimental data from Werner et al.[18] Werner et al. have also reported a DFT determination for copper up to 70 eV, which is equivalent to our own at such energies. For 0−120 eV, Hagemann's data was chiefly obtained using transmission

dx.doi.org/10.1021/jp408438r | J. Phys. Chem. A 2014, 118, 909−914

measurements on thin films, along with a Kramers−Kronig transformation algorithm, while Werner's experimental data stems from REELS analysis.

It is important to consider first the significant differences between the two experimental curves. Optical data in this energy region is particularly sparse, even for commonly studied materials such as copper, and so the significantly higher resonance peaks measured by Werner et al. and the vastly different structures around 60 eV are cause for concern regarding the reliability of the measured data. This is exacerbated by the lack of uncertainties, which is standard practice for such measurements. In addition to the absence of experimental optical data for many materials, the strong variation between different measurements here clearly demonstrates the importance of developing a theoretical benchmark.

In terms of the theoretical result, we find that although the general form of the curve is qualitatively consistent with the experimental results, absolute agreement is again quite poor in many areas. First, the theoretical determination yields a much more detailed spectrum. This is expected due to experimental broadening effects and other uncertainties not quoted for either data set, which would restrict the resolution of measurements and lead to loss of structure in the ELF. One might expect that this would have a very small effect on resulting electron IMFPs since the IMFP calculation requires an integration over a range of energies that would negate the contributions of such details.

In practice, however, the inclusion of detailed structure in the optical ELF is actually very important. Figure 2 demonstrates that DFT predicts significantly stronger losses than measured by Hagemann et al. at the main peak energies of around 20 and 28 eV, and higher losses than Werner et al. around 30 to 50 eV. Because of the restrictions from optical sum-rules,[30] extra losses in these parts of the spectrum mean lower losses at higher energies, as seen in the figure. These sum-rules are often used to check the consistency of optical data; however, they are ultimately only able to demonstrate plausibility over a wide energy range and do not constrain the detailed structure of the ELF in the small region that is our concern.

The reordering of the loss spectrum does not change the total losses overall, but it does affect the IMFP at finite energies. As discussed in the previous section, the form of eq 11 ensures that the low-energy behavior of the optical ELF has an exaggerated effect on the low-energy IMFP. This is especially true for energies where the IMFP is asymptotic.

The reliability of the theoretical result may be evaluated in an approximate fashion by consideration of the stability of the calculation with respect to a number of computational parameters. Although it is impossible to meaningfully quantify the gross theoretical error, we are able to demonstrate in Figure 3 the variation expected by weakening convergence criteria and making small changes to our physical model.

Here, we see that the result is extremely well converged with respect to the number of component plane-waves making up the LAPW computation, in addition to the maximum plane-wave momenta. The theory is more sensitive, however, to variations in muffin-tin radii and the inclusion of local orbitals in the LAPW basis. The muffin-tin radius is a nonphysical parameter, separating the regions around atomic cores from interstitial areas where electronic wave functions are represented in terms of plane waves. This radius should be set as small as possible without leakage of core-state wave functions, which are best described entirely in terms of spherical harmonics. The inclusion of local orbitals is also

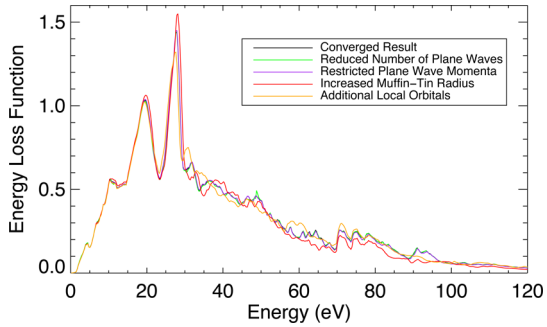

Figure 3. Optical energy loss function of copper determined using different convergence criteria and modeling within the WIEN2k implementation of density functional theory. Differences are established using 10% variations in numerical parameters, in addition to inclusion of localized basis functions for the s, p, and d orbitals.

strictly nonphysical, though in some cases can be necessary in order to describe the local form of high-energy continuum states, for use in the determination of transition matrix elements.

The uncertainties of our calculations are necessarily overestimated by Figure 3, as we have wilfully deconverged our results. However, we can propagate these variations using the maximum-variational envelope in order to obtain a maximum expected range of IMFP values following the partial-pole transform outlined in the previous section. Figure 4 shows the

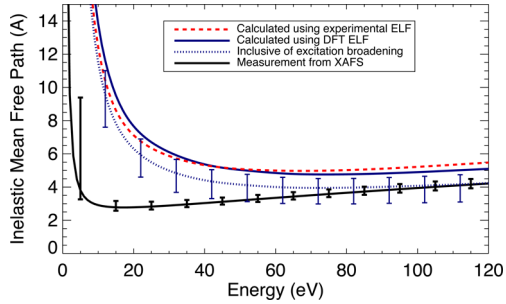

Figure 4. Electron inelastic mean free paths of copper calculated using theoretical optical loss data (solid blue curve) and measured optical loss data from Hagemann et al. (dashed red curve) compared with recent measurements using high-accuracy XAFS spectroscopy (black).[7] Also shown is a result inclusive of plasmon broadening quantified via a previous analysis of copper IMFPs (dotted blue curve),[14] along with a maximum-variational confidence interval.

electron IMFP for copper calculated using both the theoretical optical ELF of Figure 2 (solid blue curve) and the commonly used measurement from Hagemann et al.[1] (dashed red curve). A recent experimental determination of the electron IMFP using high-precision X-ray absorption fine structure (XAFS) measurements is also presented (solid black curve),[7] along with a reduced-value theoretical curve, which includes the effect of plasmon broadening following the Mermin analysis of our previous work,[14] as well as a confidence interval based on our maximum-variational analysis of the ELF from DFT.

The importance of small variations in the very low-energy region of the ELF is well illustrated. Although the clearest point of difference between the theoretical and experimental ELFs are the two extra large theory peaks at 20 and 28 eV, the theoretical IMFP actually comes in *higher* (i.e., with lower losses) than the

dx.doi.org/10.1021/jp408438r | J. Phys. Chem. A 2014, 118, 909−914

experimental result up to 45 eV. This is due to the small, but critical, difference in ELFs between 0 and 15 eV.

The two major peaks are responsible for a significant decrease in the DFT-based IMFP from around 40 eV up to the highest energies studied. This is important because it improves agreement with the IMFP extracted from XAFS. The XAFS result was considered somewhat anomalous when it was first determined, as it predicted a reduction in the IMFP of more than 20% from many theoretical tabulations given in the literature at 120 eV.[7] Herein, we demonstrate that developing the optical ELF calculated using DFT can account for a 7% reduction or up to 35% of the observed discrepancy.

The dotted blue curve indicates a reduced IMFP due to the inclusion of plasmon broadening effects, as implemented by the Mermin theory described in the previous section. The level of reduction for copper has been quantified in recent work utilizing independently proposed plasmon and single-electron excitation lifetimes.[14] This inclusion leads to a remarkably satisfying result. The dashed curve predicts electron IMFPs in excellent agreement with experimental data between 100 and 120 eV and is within the experimental uncertainty range for energies above 80 eV. This is a strong vindication of the experimental XAFS data, the modeling and extraction algorithm associated with the XAFS measurement, and also of the theoretical ELF and IMFP developments presented herein. The uncertainty presented with the theoretical curve is necessarily an overestimate but reinforces that a significant reduction from previous IMFP results is demanded not only by the recent experiment data, but by theoretical advancements as well.

Even this improved theory persists in disagreeing strongly with the experimental data for *very* low energies, up to around 40 to 50 eV. Interestingly, this problem has also been studied recently by Nagy and Echenique, who approach the theory from a rather different viewpoint in order to obtain a possible lower bound on the electron IMFP for copper in this energy range.[31] The principal concern of that work was the inclusion of the electron correlation and exchange effects, which, though present in our DFT calculations, are absent from both the Lindhard and Mermin representations of the momentum-dependent behavior of the electron ELF.

Their results produce qualitative agreement with the experimental data for energies below around 40 eV, including a reasonable prediction of the energy at which the IMFP is at a minimum. At higher energies, their lack of explicit consideration of the band structure of copper, included naturally in our model by the $|M_{n,n'}(\mathbf{k},\mathbf{q})|^2$ modulation, eventually causes the model to break down. Nevertheless, their work suggests that further understanding of exchange and correlation effects may be significant in the current discrepancies at very low electron energies, and provides a useful complementary approach, albeit one that is currently incompatible with our own.

CONCLUSIONS

The many-pole dielectric theory has been developed to find good agreement with experimental IMFPs for copper at energies above 80 eV. The inclusion of necessary physical effects due to finite plasmon resonance widths and consideration of theoretical optical losses via DFT resolves the apparent five standard error discrepancy between longstanding literature theory and recently published experimental work. Further, the coupling of DFT results with developments in many-pole dielectric theory for the determination of momentum-dependent electron ELFs without need for experimental optical data is an important advancement in its own right, aiding the investigation of optical and electron energy loss functions and electron inelastic mean free paths, and of related critical parameters in electron microscopy, X-ray optics, and condensed matter theory.

Our results demonstrate that the use of partial- or many-pole theories allows us to exploit the significantly more detailed loss spectra obtainable via DFT analysis, consequently enabling finer interrogation of experimental modeling and analysis techniques, with particular reference in this work to recently developed XAFS measurements of IMFPs. These considerations are readily applicable to any periodic condensed matter system, suggesting a plethora of investigations previously unavailable due to reliance on experimental optical data, which may be unavailable or unreliable, particularly at energies in the critical plasmon-excitation region below 120 eV.

Finally, the comparison of our results with XAFS-based measurements provides insight into the fundamental physical processes responsible for observed differences between theory and experiment. We have been able to demonstrate the applicable energy range and potential magnitude of IMFP dependence on the detailed form of the optical ELF for copper. We have also shown the energy range of importance for plasmon broadening effects, and with reference to other recently published work,[31] it can be seen that these effects are complementary to, and distinguishable from, potential changes in IMFP due to considerations of electron exchange and correlation.

AUTHOR INFORMATION

Corresponding Author

*(C.T.C.) E-mail: chantler@unimelb.edu.au. Phone: +61383445437.

Notes

The authors declare no competing financial interest.

ACKNOWLEDGMENTS

The authors acknowledge Y. Joly, the team at Melbourne, and the ANBF, APS, and AS grants for their helpful contributions to this research.

REFERENCES

(1) Hagemann, H.-J.; Gudat, W.; Kunz, C. Deutsches Elektronen-synchrontron Report SR-74/7, 1974. www.desy.de.

(2) Palik, E. D. *Handbook of Optical Constants of Solids III*; Academic Press: New York, 1998.

(3) Wallart, X.; de Villeneuve, C. H.; Allongue, P. Truly Quantitative XPS Characterization of Organic Monolayers on Silicon: Study of Alkyl and Alkoxy Monolayers on H-Si(111). *J. Am. Chem. Soc.* **2005**, *127*, 7871−7878.

(4) Werner, W. S. M.; Smekal, W.; Stori, H.; Winter, H.; Stefani, G.; Ruocco, A.; Offi, F.; Got-ter, R.; Morgante, A.; Tommasini, F. Emission-Depth-Selective Auger Photoelectron Coincidence Spectroscopy. *Phys. Rev. Lett.* **2005**, *94*, 038302−038305.

(5) Cumpson, P. J. Elastic Scattering Corrections in AES and XPS. III. Behaviour of Electron Transport Mean Free Path in Solids for Kinetic Energies in the Range 100 eV < *E* <400 eV. *Surf. Interface Anal.* **1997**, *25*, 447−453.

(6) Kimoto, K.; Asaka, T.; Nagai, T.; Saito, M.; Matsui, Y.; Ishizuka, K. Element-Selective Imaging of Atomic Columns in a Crystal Using STEM and EELS. *Nature* **2007**, *450*, 702−704.

(7) Bourke, J. D.; Chantler, C. T. Measurements of Electron Inelastic Mean Free Paths in Materials. *Phys. Rev. Lett.* **2010**, *104*, 206601(1−4).

(8) Chantler, C. T.; Bourke, J. D. X-ray Spectroscopic Measurement of Photoelectron Inelastic Mean Free Paths in Molybdenum. *J. Phys. Chem. Lett.* **2010**, *1*, 2422−2427.
(9) de Jonge, M. D.; Tran, C. Q.; Chantler, C. T.; Barnea, Z.; Dhal, B. B.; Cookson, D. J.; Lee, W.; Mashayekhi, A. Measurement of the X-ray Mass Attenuation Coefficient and Determination of the Imaginary Component of the Atomic Form Factor of Molybdenum Over the 13.5 −41.5 keV Energy Range. *Phys. Rev. A* **2005**, *71*, 032702(1−16).
(10) Chantler, C. T.; Rae, N. A.; Islam, M. T.; Best, S. P.; Yeo, J.; Smale, L. F.; Hester, J.; Mohammad, N.; Wang, F. Stereochemical Analysis of Ferrocene and the Uncertainty of Fluorescence XAFS Data. *J. Synch. Radiat.* **2012**, *19*, 145−158.
(11) Glover, J. L.; Chantler, C. T.; Soldatov, A. V.; Smolentsev, G.; Feiters, M. C. Theoretical XANES Study of the Activated Nickel (*t*-Amylisocyanide) Molecule. *AIP Conf. Proc.* **2007**, *882*, 625−627.
(12) Bourke, J. D.; Chantler, C. T.; Witte, C. Finite Difference Method Calculations of X-ray Absorption Fine Structure for Copper. *Phys. Lett. A* **2007**, *360*, 702−706.
(13) Zdyb, R.; Mentes, T. O.; Locatelli, A.; Nino, M. A.; Bauer, E. Inelastic Mean Free Path From Reflectivity of Slow Electrons. *Phys. Rev. B* **2013**, *87*, 075436(1−5).
(14) Bourke, J. D.; Chantler, C. T. Electron Energy Loss Spectra and Overestimation of Inelastic Mean Free Paths in Many-Pole Models. *J. Phys. Chem. A* **2012**, *116*, 3202−3205.
(15) Tanuma, S.; Powell, C. J.; Penn, D. R. Calculations of Electron Inelastic Mean Free Paths. II. Data for 27 Elements Over the 50−2000 eV range. *Surf. Interface Anal.* **1991**, *17*, 911−926.
(16) Sorini, A. P.; Kas, J. J.; Rehr, J. J.; Prange, M. P.; Levine, Z. H. Ab Initio Calculations of Electron Inelastic Mean Free Paths and Stopping Powers. *Phys. Rev. B* **2008**, *74*, 165111(1−8).
(17) Abril, I.; Garcia-Molina, R.; Denton, C. D.; Perez-Perez, F. J.; Arista, N. R. Dielectric De-scription of Wakes and Stopping Powers in Solids. *Phys. Rev. A* **1998**, *58*, 357−366.
(18) Werner, W. S. M.; Glantschnig, K.; Ambrosch-Draxl, C. Optical Constants and Inelastic Electron-Scattering Data for 17 Elemental Metals. *J. Phys. Chem. Ref. Data* **2009**, *38*, 1013−1092.
(19) Tanuma, S.; Powell, C. J.; Penn, D. R. Calculations of Electron Inelastic Mean Free Paths. IX. Data for 41 Elemental Solids Over the 50 eV to 30 keV Range. *Surf. Interface Anal.* **2011**, *43*, 689−713.
(20) Hohenberg, P.; Kohn, W. Inhomogeneous Electron Gas. *Phys. Rev.* **1964**, *136*, B864−B871.
(21) Parr, R. G. Density Functional Theory. *Annu. Rev. Phys. Chem.* **1983**, *34*, 631−656.
(22) Kohn, W.; Sham, L. J. Self-Consistent Equations Including Exchange and Correlation Effects. *Phys. Rev.* **1965**, *140*, A1133−A1138.
(23) Blaha, P.; Schwarz, K.; Madsen, G. K. H.; Kvasnicka, D.; Luitz, J. *WIEN2k: An Augmented Plane Wave Plus Local Orbitals Program for Calculating Crystal Properties*; Vienna University of Technology: Vienna, Austria, 2001.
(24) Perdew, J. P.; Burke, S.; Ernzerhof, M. Generalized Gradient Approximation Made Simple. *Phys. Rev. Lett.* **1996**, *77*, 3865−3868.
(25) Ambrosch-Draxl, C.; Sofo, J. O. Linear Optical Properties of Solids Within the Full-Potential Linearized Augmented Planewave Method. *Comput. Phys. Commun.* **2006**, *175*, 1−14.
(26) Lindhard, J. On the Properties of a Gas of Charged Particles. *Dan. Mat. Fys. Medd.* **1954**, *28*, 8.
(27) Penn, D. R. Electron Mean-Free-Path Calculations Using a Model Dielectric Function. *Phys. Rev. B* **1987**, *35*, 482−486.
(28) Tung, C. J.; Ashley, J. C.; Ritchie, R. H. Electron Inelastic Mean Free Paths and Energy Losses in Solids II. *Surf. Sci.* **1979**, *81*, 427−439.
(29) Mermin, N. D. Lindhard Dielectric Function in the Relaxation-Time Approximation. *Phys. Rev. B* **1970**, *1*, 2362.
(30) Smith, D. Y.; Shiles, E. Finite-Energy *f*-Sum Rules for Valence Electrons. *Phys. Rev. B* **1978**, *17*, 4689−4694.
(31) Nagy, I.; Echenique, P. M. Mean Free Path of a Suddenly Created Fast Electron Moving in a Degenerate Electron Gas. *Phys. Rev. B* **2012**, *85*, 115131(1−4).